Title:

Neural reinstatement reveals divided organization of fear and extinction memories in the human brain

Authors:

Augustin C. Hennings[1,2], Mason McClay[3], Michael R. Drew[1,2], Jarrod A. Lewis-Peacock[1,2,4,5], Joseph E. Dunsmoor*[1,2,5]

Affiliations:

1. Institute for Neuroscience, University of Texas at Austin, Austin, TX, USA
2. Center for Learning and Memory, Department of Neuroscience, University of Texas at Austin, Austin, TX, USA
3. Department of Psychology, University of California, Los Angeles, CA, USA
4. Department of Psychology, University of Texas at Austin, Austin, TX, USA
5. Department of Psychiatry, Dell Medical School, University of Texas at Austin, Austin, TX, USA

*Correspondence to joseph.dunsmoor@austin.utexas.edu

17

Summary

Neurobiological research in rodents has revealed that competing experiences of fear and extinction are stored as distinct memory traces in the brain. This divided organization is adaptive for mitigating overgeneralization of fear to related stimuli that are learned to be safe, while also maintaining threat associations for unsafe stimuli. Whether a similar division exists in the human brain remains unclear. Here, we used a hybrid form of Pavlovian conditioning with an episodic memory component to identify overlapping multivariate patterns of fMRI activity associated with the formation and retrieval of fear versus extinction. In healthy adults, distinct regions of the medial PFC and hippocampus showed selective neural coding for fear and extinction memories. This dissociation was absent in participants with PTSD symptoms. The divided neural organization of fear and extinction may support flexible retrieval of context-appropriate emotional memories, while their disorganization may promote overgeneralization and increased fear relapse in affective disorders.

31

32

Introduction

Maintaining separate and competing memories of threat and safety is key to adaptive behavior. The inability to maintain memories of safety to overcome threat associations is characteristic of affective disorders such as posttraumatic stress disorder (PTSD) (Lissek and van Meurs, 2015; Pitman et al., 2012). Neurobiological research using Pavlovian conditioning as a model shows that neural ensembles within and between dissociable regions organize the encoding, storage, and retrieval of fear (threat) and extinction (safety) memory (Johansen et al., 2011; Liu et al., 2012; Rashid et al., 2016; Tovote et al., 2015). This research confirms early theories—dating back to the time of Pavlov—that extinction is an active learning process that generates a secondary memory of safety for a particular stimulus that is stored in parallel to the memory of fear for that stimulus. In the rodent brain, these memory traces can be separated into discrete neural ensembles with distinct pathways between regions of the medial temporal lobe (MTL) and subdivisions of the medial prefrontal cortex (mPFC) (Davis et al., 2017; Giustino and Maren, 2015; Herry et al., 2008; Senn et al., 2014; Sierra-Mercado et al., 2011). Whether a similar neural organization exists in the human brain, whereby fear and extinction memories are segregated into separate neural regions, is unclear. Here, we use multivariate pattern analysis (MVPA) of functional magnetic resonance imaging (fMRI) data to isolate spatially distributed patterns of overlapping network activity unique to the encoding and retrieval of fear versus extinction memories. We compare these neural signatures between healthy adults and individuals with PTSD symptoms, for which the ability to organize separable fear and extinction memories is presumably abnormal (Milad and Quirk, 2012).

Identifying quantifiable memory traces in the brain can be challenging: memory representations are widely distributed within and across discrete brain regions, memories change over time, and not all experiences induce a persistent change in the brain. Fear conditioning is an ideal model to investigate the neural representations of memory, as it rapidly induces a stable

and persistent associative memory with an objective behavioral correlate. One of the most important discoveries in the neuroscience of associative learning has been the localization of neural circuits selective for the formation and retrieval of fear versus extinction memory. In the MTL, sparse coding allows for fear and extinction to exist simultaneously in the same structures (Frankland et al., 2019; Josselyn et al., 2015), while a more stark division exists in the mPFC. The prelimbic cortex, homologous to the human dorsal anterior cingulate cortex (dACC), is activated during learning and retrieval of fear associations (Burgos-Robles et al., 2009, 2017; Sotres-Bayon et al., 2012), whereas the infralimbic cortex, homologous to the human ventromedial PFC (vmPFC), is a critical site of extinction memory formation and retrieval (Do-Monte et al., 2015; Klavir et al., 2017; Milad and Quirk, 2002). These areas interact dynamically with the amygdala and hippocampus to either express or suppress conditioned fear (Marek et al., 2018; Senn et al., 2014).

Human neuroimaging has successfully translated evidence from rodents that the dACC is among the most consistently active regions during fear conditioning (Fullana et al., 2016). However, it is far less clear in humans whether this region is also the site of long-term storage and retrieval of the acquired fear memories. Moreover, neuroimaging evidence of vmPFC involvement in extinction is surprisingly scant. Indeed, meta-analyses show the vmPFC is *not* among a collection of regions active during extinction learning (Fullana et al., 2018). This inconsistency between animal neurophysiology and human neuroimaging has been a puzzle and limits the translational utility of advances in extinction research from rodents to humans.

A major hurdle to translating animal neurophysiology to human neuroimaging is a methodology to "label" brain activity uniquely associated with memories of either fear or extinction. In rodents, state-of-the-art advances in activity-dependent labeling can separate these memory traces by measuring the overlap in neuronal activity during acquisition and retrieval in collections of neurons, termed engrams (Frankland et al., 2019; Lacagnina et al., 2019). An analogous

83   analytic approach in human neuroimaging involves correlating overlapping multivariate patterns

84   of brain activity during memory encoding and retrieval. The match between patterns of activity in

85   distributed voxels during encoding and retrieval provides an index of memory fidelity, albeit not at

86   the cellular level. This neuroimaging technique has been widely applied to the study of human

87   episodic memory (Johnson et al., 2009; Polyn et al., 2005; Ritchey et al., 2013; Staresina et al.,

88   2012; Staudigl et al., 2015). Whether this technique can be leveraged to isolate associative

89   memory traces of fear and extinction in the human brain has not been tested.

90   Here, we use a two-day hybrid conditioning/episodic memory design that incorporates

91   trial-unique (i.e., non-repeating) semantic exemplars as conditioned stimuli (CS) during fear

92   conditioning and extinction on day 1 (Dunsmoor and Kroes, 2019). On day 2, participants undergo

93   a memory test composed of the unique CS exemplars encoded during both conditioning and

94   extinction. This hybrid design overcomes an inherent obstacle to the typical conditioning protocol.

95   That is, typically the same CS (e.g., a colored shape) is repeated across all experimental phases.

96   Consequently, it is only possible to measure retrieval of either the putative fear or extinction

97   memory at test, but not both. In our hybrid design we simultaneously isolate specific episodes

98   associated with fear and extinction (comparable to activity-dependent labeling in murine studies)

99   and quantify the overlap in patterns of activity for each CS as a function of the temporal context

100   in which the CS was encoded. In this way, we can quantify whether and how these competing

101   memories are distinctly organized in separable patterns of activity in a given participant and in a

102   single experiment. This design innovation allows us to leverage technical advances in multivariate

103   neuroimaging of human episodic memory within the conceptual framework of functional labeling

104   from rodent neurophysiology.

105   We hypothesized that the healthy adult brain organizes and maintains separable

106   mnemonic representations of fear and extinction, and we sought to distinguish these memories

107   based on the temporal context in which the memory was originally formed. We hypothesized that

108   fear memories would be represented similarly in healthy adults and individuals with post-traumatic

109   stress symptoms (PTSS). However, based on extensive evidence of maladaptive return of fear in

110   PTSD, we hypothesized that neural organization of extinction memories would differ between

111   groups.

112   **RESULTS**

113   **Fig. 1** provides an overview of the study procedures and analytic approach. Each subject

114   encoded trial-unique pictures of animals and tools before, during, and after fear conditioning. One

115   semantic category (animals or tools, counterbalanced) served as CS+ and co-terminated with an

116   electrical shock on 50% of trials during fear conditioning, while the other category never paired

117   with shock (CS-). Extinction learning immediately followed fear conditioning, during which no

118   shocks were delivered. Participants returned 24-hours later for a surprise recognition memory test

119   comprised of the CSs from each phase plus novel lures.

120
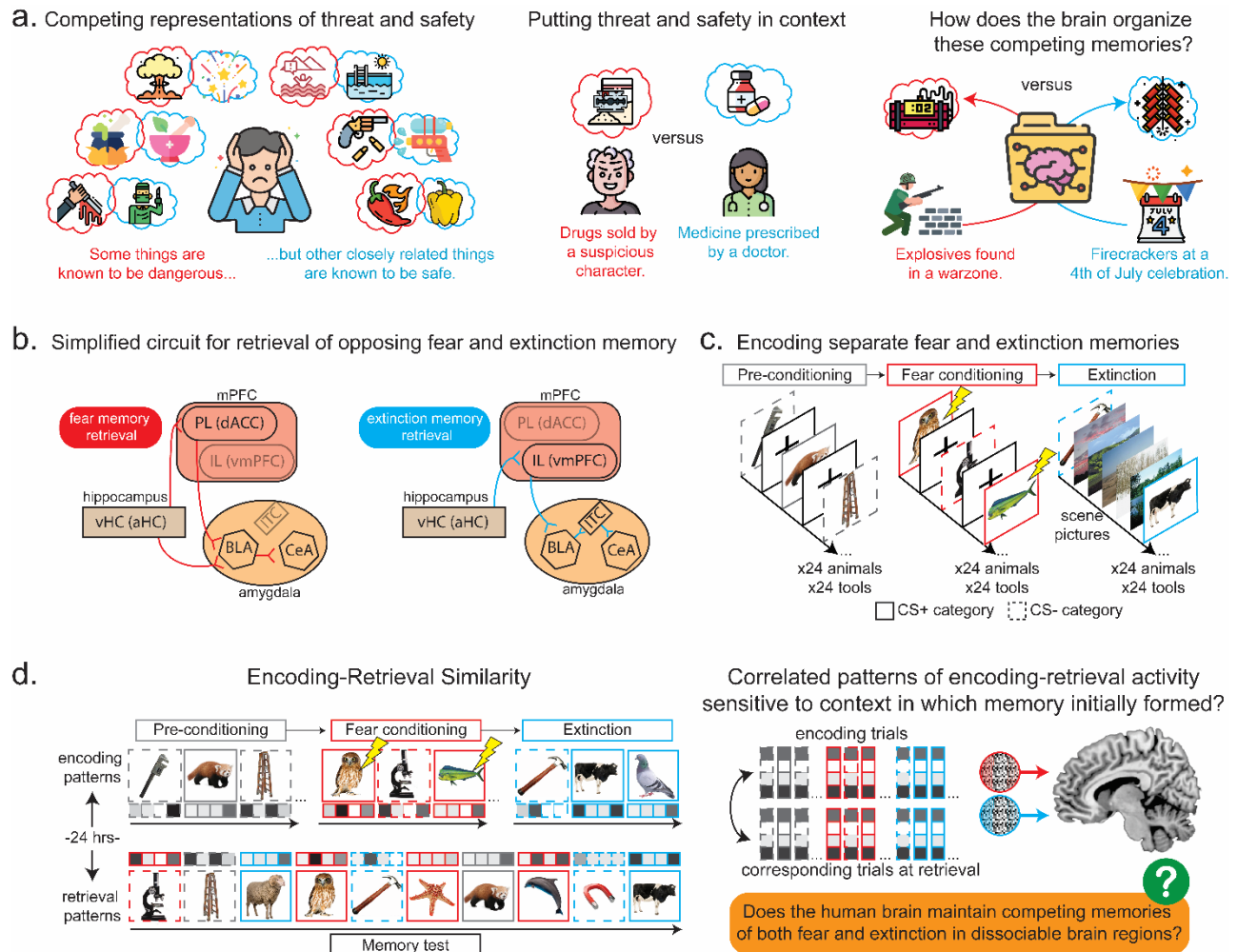
Figure 1. Divided organization of fear and extinction memories in the human brain. **a. Schematic overview.** People maintain competing representations of threat and safety for closely related stimuli or situations. We can often retrieve the appropriate associative memory given the context. How the brain organizes these competing memories remains an important question, as disorganization between them may lead to maladaptive fear and anxiety in harmless situations. **b. Simplified circuits diagrams** of fear and extinction memory retrieval, highlighting the interactions between the MTL and mPFC. Human homologues of neural structures in rodents are given in parentheses. **c. Overview of the associative learning task on Day 1.** Semantic categories of images served as the CS+/-, each trial was a unique category exemplar that did not repeat. During fear conditioning, 50% of the CS+s co-terminated with a mild electric shock (US). During extinction learning, a stream of natural scene images appeared between CSs (see Hennings et al., 2020). **d. Overview of the encoding-retrieval similarity analysis.** 24-hrs after associative learning, participants were placed back into the scanner and completed a surprise recognition memory test. To test for neural reinstatement within a given ROI, the item-specific pattern of fMRI activity elicited by each CS was correlated with the activity pattern from when that item was initially encoded. MTL: medial temporal lobe; mPFC medial prefrontal cortex; PL: prelimbic cortex; IL: infralimbic cortex; vHC: ventral hippocampus; dACC: dorsal anterior cingulate cortex; vmPFC: ventromedial prefrontal cortex; aHC: anterior hippocampus; BLA: basolateral amygdala; ITC: intercalated cells; CeA: central nucleus of the amygdala.
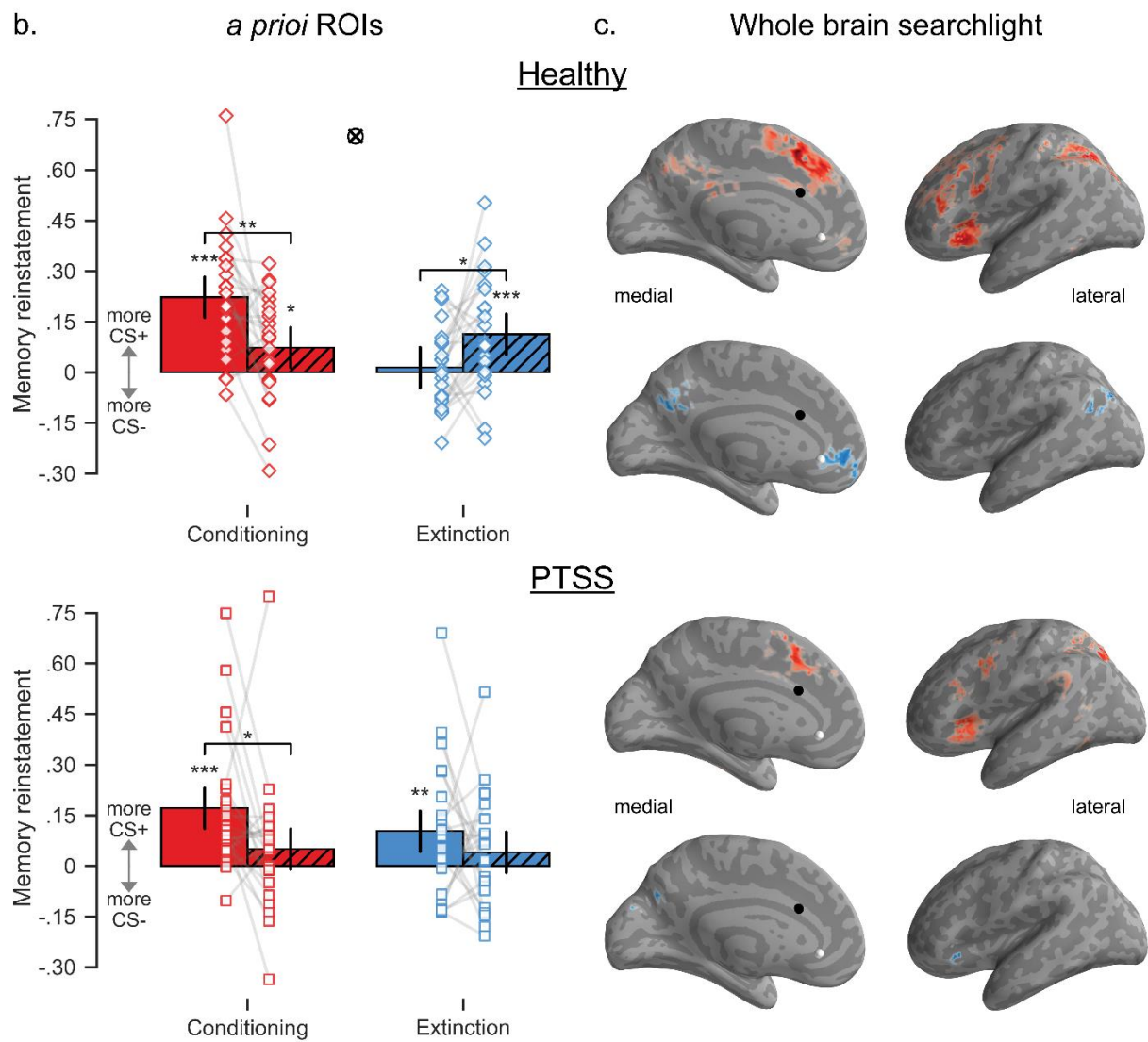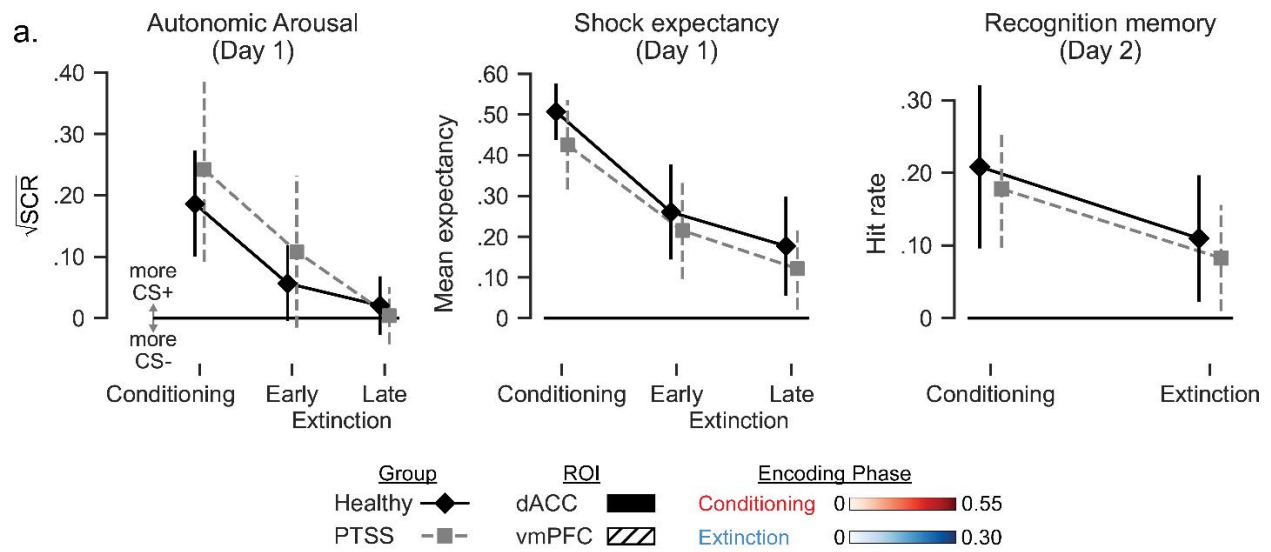
Behavioral results

Explicit and implicit measures of learning. As we previously reported (Hennings et al., 2020), the success of fear conditioning and extinction learning was assessed by skin conductance responses (SCR) and trial-by-trial shock expectancy (Yes/No 2-alternative forced choice; AFC). Analyses focused on differential responding (i.e., CS+ > CS- differences) in SCR and shock expectancy from each phase (**Fig. 2a**). During conditioning, both healthy adults and individuals with PTSS exhibited significant CS+ > CS- responses for both SCR (Healthy: $t_{(23)}$ = 4.22, P = 3.25e-4; PTSS: $t_{(23)}$ = 3.17, P = 4.31e-3) and shock expectancy (Healthy: $t_{(23)}$ = 14.3, P = 6.16e-13; PTSS: $t_{(23)}$ = 7.62, P = 9.89e-8). The success of extinction learning was assessed by comparing differential responses from conditioning to the second half of extinction ("late extinction"). Both groups displayed a significant reduction in differential SCR (Healthy: $t_{(21)}$ = -2.6, P = 0.017; PTSS: $t_{(21)}$ = -2.86, P = 9.34e-3) and shock expectancy (Healthy: $t_{(23)}$ = -4.33, P = 2.46e-4; PTSS: $t_{(23)}$ = -3.66, P = 1.29e-3) between these two phases. Importantly, there were no significant differences in behavioral responses between healthy participants and participants with PTSS during either conditioning (SCR: $t_{(46)}$ = 0.63, P = 0.53; expectancy: $t_{(46)}$ = 1.23, P = 0.22) or late extinction (SCR: $t_{(42)}$ = 0.49, P = 0.63; expectancy: $t_{(46)}$ = 0.69, P = 0.50). Together these results demonstrate successful and equivalent fear conditioning and within-session extinction in both groups.

Recognition memory. Overall, performance on the recognition memory test replicated previous behavioral findings (Dunsmoor et al., 2015a, 2018; Keller and Dunsmoor, 2020), in that memory was better for CS+ items compared to CS- from all phases, and overall higher for conditioning compared to other phases. Here, we report an analysis of high confidence hit rates with the purpose of testing for a difference in episodic memory performance between healthy adults and individuals with PTSS. A mixed-effects ANOVA of high confidence hit rates revealed no significant main effect of *group* ($F_{1, 46}$ = 1.37, P = 0.25), and no significant two-way interactions

166   between *group* and either *CS type* or *encoding context,* and no significant three-way interaction

167   (All Ps ≥ 0.44). These results indicate that explicit recognition memory for the CS items was not

168   different between groups.

169

a.

Autonomic Arousal (Day 1)
Shock expectancy (Day 1)
Recognition memory (Day 2)

Group
Healthy ◆
PTSS ■ (dashed)

ROI
dACC ■
vmPFC ▨

Encoding Phase
Conditioning 0 — 0.55
Extinction 0 — 0.30

b. *a prioi* ROIs   c. Whole brain searchlight

Healthy

PTSS

medial   lateral

170

Figure 2. Dissociable reinstatement of emotional memories. All error bars correspond to the 95% confidence interval of the CS+ – CS- difference. ***P < 0.001, **P < 0.01, *P < 0.05, FDR corrected. **a. Behavioral responses.** Autonomic arousal and explicit shock expectancy from fear conditioning and extinction (split by half) on Day 1 are replicated from Hennings et al., 2020. Results show successful acquisition and extinction of differential (CS+ > CS-) responses for both SCR and shock expectancy for both groups. 24hr delayed recognition memory hit rates are shown for items encoded during learning. Critically, no group differences were observed in behavioral responses during associative learning or the recognition memory test. See text for statistical analyses. **b. Reinstatement in *a priori* ROIs.** *Top.* Healthy adults exhibited a significant double dissociation of emotional reinstatement in the mPFC, such that reinstatement for items encoded during conditioning was higher in the dACC, and extinction reinstatement was higher in the vmPFC. *Bottom.* In adults with PTSS, the dACC displayed significant emotional reinstatement of items encoded during both conditioning and extinction, revealing a misallocation of extinction memories. **B. Whole brain analysis.** A searchlight was run over the entire brain, calculating reinstatement in each location. Medial and lateral views of the inflated left hemisphere are shown; results were qualitatively similar across hemispheres. The heatmaps show average CS+ – CS- reinstatement for items from conditioning (red) and from extinction (blue). Maps were threshold at P < 0.001 one-sided for CS+ > CS- with a cluster-wise threshold (FWE) of P < 0.05. The centers of *a priori* ROIs are marked on the cortical surface for the dACC (black) and vmPFC (white).

Emotional memory reinstatement in the medial prefrontal cortex

The analysis here focuses on the overlap of multi-voxel fMRI activity patterns of items from encoding to retrieval (i.e., encoding retrieval similarity), irrespective of memory performance. The voxel-wise patterns of activity elicited by each CS item during the recognition memory test was correlated with the patterns of activity elicited by those same CS items when they were initially encoded during either the pre-conditioning, fear conditioning, or extinction phase. To control for item-level reinstatement effects, these correlations were Fisher z-transformed and then the average correlation of CS- trials was subtracted from the average correlation of the CS+ trials from the same encoding context. This analysis focused on two distinct subregions of the mPFC motivated by rodent work (Burgos-Robles et al., 2017; Do-Monte et al., 2015): the dACC and vmPFC. These regions were defined by drawing spheres around *a priori* peak activations (see **Online Methods**).

In healthy adults, the dACC exhibited selective reinstatement for CS+ items (compared to CS- items) that were encoded during fear conditioning (**Fig. 2b, top**; difference = 0.22, 95% CI = [0.16, 0.28], P_{FDR} = 4.62e-12). This finding accords with rodent models that show the PL is

205 involved in both the learning and retrieval of long-term fear memories. Selective reinstatement in

206 the dACC was stronger for fear memories (CS+ – CS- from conditioning) than for extinction

207 memories (CS+ – CS- from extinction; 0.21, [0.12, 0.29], P_{FDR} = 6.26e-6). Moreover, this region

208 did not show any selective reinstatement of extinction memories (0.014, [-0.046, 0.075], P_{FDR} =

209 0.64) or pre-conditioning memories (0.006, [-0.054, 0.066], P_{FDR} = 0.84). In sum, the dACC

210 appears highly specialized for the reinstatement of fear memories in the healthy adult brain. In

211 the vmPFC, there was selective reinstatement for both fear memories (0.074, [0.013, 0.134], P_{FDR}

212 = 0.033) and extinction memories (0.113, [0.053, 0.173], P_{FDR} = 9.20e-4). There was no selective

213 reinstatement of pre-conditioning memories (-0.020, [-0.081, 0.040], P_{FDR} = 0.50). Notably, there

214 was a significant double dissociation in the selective reinstatement of fear and extinction

215 memories between these two regions (significant *CS type * encoding context * ROI* interaction;

216 $X^2_{(1)}$ = 16.2, P = 5.71e-5). Specifically, there was stronger reinstatement of fear memories in the

217 dACC relative to the vmPFC (0.149, [0.064, 0.234], P_{FDR} = 0.002), and stronger reinstatement of

218 extinction memories in the vmPFC relative to the dACC (0.099, [0.014, 0.184], P_{FDR} = 0.031).

219 Altogether, in healthy adults, discrete regions of the mPFC exhibited a double dissociation in the

220 selective reinstatement of fear memories and extinction memories, as identified by the temporal

221 context in which the memories were formed.

222   As with healthy adults, individuals with PTSS also exhibited selective reinstatement of

223 CS+ items in the dACC for items encoded during conditioning (**Fig. 2b**, bottom; 0.171, [0.111,

224 0.231], P_{FDR} = 1.53e-7), and reinstatement of fear memories was stronger in the dACC relative to

225 the vmPFC (0.121, [0.036, 0.206], P_{FDR} = 0.011). The dACC also did not exhibit selective

226 reinstatement for pre-conditioning memories (0.032, [-0.028, 0.092], P_{FDR} = 0.30). This pattern of

227 selective fear memory reinstatement is consistent with results in healthy adults and suggests that

228 individuals with PTSS do not exhibit a fear processing related deficit. Unlike the healthy adult

229 group, however, the PTSS group also showed selective reinstatement for CS+ items encoded

230   during extinction in the dACC (0.103, [0.043, 0.164], P_{FDR} = 0.002). These results suggest that

231   individuals with PTSS are misallocating extinction memories, as information encoded in the

232   extinction context was reinstated in the same region involved in the formation and retrieval of fear

233   memories. In the vmPFC, there was unexpected selectivity for CS- items encoded prior to fear

234   conditioning (-0.079, [-0.139, -0.019], P_{FDR} = 0.024). In contrast to the healthy adult group, there

235   was no evidence of selective reinstatement for CS+ items encoded during either conditioning

236   (0.050, [-0.010, 0.110, P_{FDR} = 0.10) or extinction (0.041, [-0.020, 0.101], P_{FDR} = 0.19) in the

237   vmPFC. The significant double dissociation of fear and extinction memory reinstatement we

238   observed in the healthy adults was not present in the PTSS group (no significant *CS type **

239   *encoding context * ROI* interaction; $X^2_{(1)}$ = 0.88, P = 0.35). Thus, while individuals with PTSS

240   exhibit normal reinstatement of fear memories in the dACC, this group did not exhibit any selective

241   reinstatement of CS+ memories in the vmPFC. Instead, extinction memory reinstatement was

242   misallocated to the dACC.

243   **Emotional memory reinstatement outside *a priori* cortical ROIs**

244   To complement the results from the *a priori* ROIs, we conducted an exploratory whole

245   brain searchlight for selective CS+ reinstatement (**Fig. 2c**). In healthy adults, this analysis

246   revealed additional brain regions exhibiting selective reinstatement of fear and extinction

247   memories (See **Supplementary Table 1** for full list of cluster locations). In addition to the dACC,

248   we found that fear memories were reinstated in the anterior insula, a region consistently

249   implicated in human fear memory (Fullana et al., 2016). For the reinstatement of extinction

250   memories, the largest cluster was found in vmPFC. Other cortical regions including the medial

251   frontal gyrus and precuneus exhibited selective reinstatement for both fear and extinction

252   memories. Individuals with PTSS were similar to healthy adults with the reinstatement of fear

253   memories in large clusters corresponding to the dACC, bilateral insula, and other cortical regions.

254   For extinction memories, we observed significant clusters in the cuneus, as well as in bilateral

255   insula. It is interesting that the insula showed significant reinstatement for extinction items, as this

256   region selectively reinstated fear memories in healthy adults.

257   **Emotional memory reinstatement in the medial temporal lobe**

258   Previous work has shown that the amygdala and hippocampus are core components of

259   neurocircuitry involved in the acquisition and retrieval of both fear and extinction memories. The

260   hippocampus in particular exerts contextual control over memory retrieval (Maren et al., 2013).

261   Emerging neurobiological models in rodents indicate that different subfields along the long-axis

262   of the hippocampus serve discrete functions in the course of conditioning and extinction (Bast et

263   al., 2003; Corcoran et al., 2005; Marek et al., 2018; Meyer et al., 2019; Qin et al., 2021; Ye et al.,

264   2017). Human neuroimaging also shows functional specializations for these subfields in memory

265   and affective processes (Cooper and Ritchey, 2019; Meyer et al., 2019; Poppenk et al., 2013).

266   Using subject-specific anatomical segmentations, we probed emotional memory reinstatement

267   along the long-axis of the hippocampus in three bi-lateral subfields: head (anterior; aHC), body,

268   and tail (posterior; pHC). The amygdala was similarly segmented into two bilateral ROIs known

269   to have functional specialization in conditioning and extinction processes: the basolateral

270   amygdala (BLA) and the central nucleus of the amygdala (CeM) (Pape and Pare, 2010).

271   *Hippocampus.* No selective reinstatement of CS+ items was observed for items from any

272   encoding context in any hippocampal subfield in either healthy adults or those with PTSS (all P_{FDR}

273   ≥ 0.45). However, a linear-mixed effects model revealed a significant three-way interaction of

274   *encoding context * subfield * group* ($X^2_{(4)}$ = 12.8, P = 0.012; see **Online Methods** for full model

275   specification). The significance of this term suggests that subfields of the hippocampus may be

276   sensitive to encoding context in general, but not CS type. As such, we probed reinstatement by

277   encoding context, collapsing across CS+/-. In both groups, the pHC selectively reinstated items

278   from the fear conditioning context. In healthy adults, reinstatement of fear memories was stronger

279   than reinstatement of extinction memories (4.36e-2, [1.40e-2, 7.32e-2], P_{FDR} = 0.019), whereas in

14

280   adults with PTSS, it was stronger than both extinction memories (4.33e-2, [1.36e-2, 7.29e-2], P_{FDR}

281   = 0.019) and pre-conditioning memories (4.41e-2, [1.45e-2, 7.37e-2], P_{FDR} = 0.019). The body of

282   the hippocampus did not show reinstatement specific to any encoding context (all phase

283   comparisons $P_{FDR} \geq 0.11$). In contrast to the pHC, the aHC portion selectively reinstated items

284   from extinction more than items from conditioning (0.065, [0.035, 0.094], P_{FDR} = 3.36e-4), although

285   this was only observed in healthy adults. These results suggest a gradient of functional

286   specialization along the long axis of the hippocampus.

287   We directly tested the dissociation between the aHC and pHC subfields and found a

288   significant double dissociation in healthy adults (significant *encoding context * subfield* interaction;

289   $X^2_{(1)}$ = 23.04, P = 1.59e-6). Specifically, the pHC exhibited more fear memory reinstatement than

290   the aHC (0.033, [0.003, 0.063], P_{FDR} = 0.038), and the aHC exhibited more extinction memory

291   reinstatement than the pHC (0.075, [0.046, 0.105], P_{FDR} = 2.51e-6). (**Fig. 3**). This double

292   dissociation was not observed in the PTSS group (no significant *encoding context * subfield*

293   interaction; $X^2_{(1)}$ = 1.80, P = 0.19). In these participants, fear memories were biased towards the

294   pHC (0.034, [0.004, 0.063], P_{FDR} = 0.038), but there was no preference between the aHC and

295   pHC for extinction memories (-0.004, [-0.034, 0.026], P_{FDR} = 0.80). The lack of extinction

296   reinstatement in the aHC further supports the idea that the neural organization of safety memories

297   is dysregulated in PTSS as compared to healthy adults.
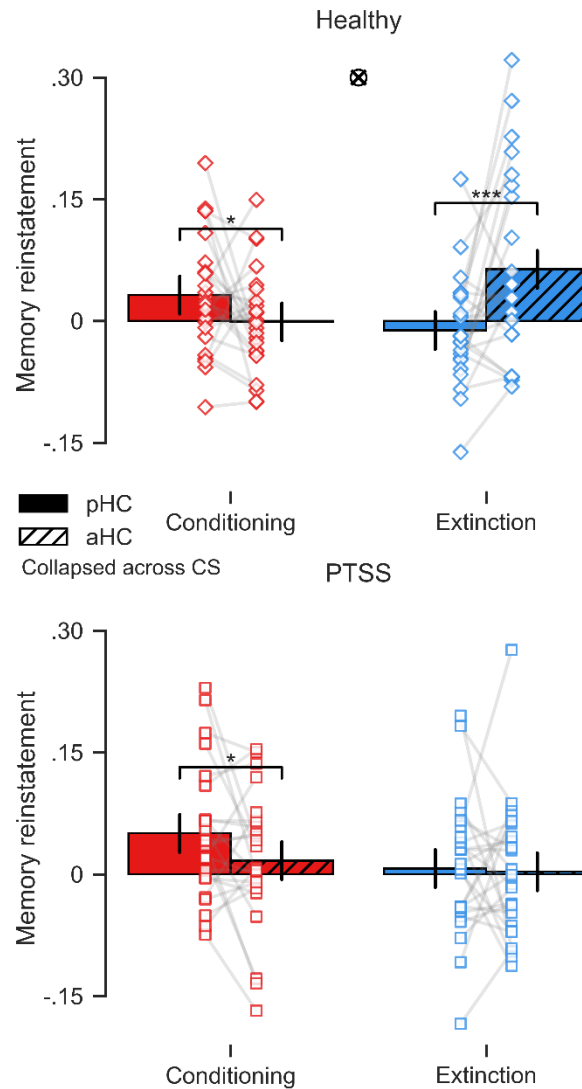
Figure 3. Differential reinstatement of emotional memories along the long axis of the hippocampus. Reinstatement was collapsed across CS+/- by encoding context in each long-axis subfield of the hippocampus. Error bars correspond to the 95% confidence interval of the marginal means. Phase specific reinstatement was observed in the pHC and aHC subfields, but not the body of the hippocampus (data not shown). ***P < 0.001, *P < 0.05 FDR corrected. *Top.* Healthy adults exhibited a double dissociation of reinstatement in the hippocampus, such that reinstatement for items encoded during conditioning was higher in the pHC, and extinction reinstatement was higher in the aHC. *Bottom*. In adults with PTSS, the pHC subfield exhibited more reinstatement of conditioning items than the aHC.

Amygdala. We also examined whether subfields of the amygdala exhibited selective

reinstatement of CS+ items, however none was observed for any encoding context in any subfield,

in either healthy adults or those with PTSS (all $P_{FDR} \geq 0.64$). In addition, we did not observe any

16

311   significant main effects or interactions in a linear mixed-effects model, and thus did not perform

312   any other follow-up tests.

313   **MTL activity at retrieval predicts dissociable reinstatement in the mPFC.**

314   *Univariate activity.* Our *a priori* analysis in the mPFC showed that healthy adults exhibited

315   a double dissociation of emotional memory reinstatement. What determines in which area of the

316   mPFC a particular item is reinstated? The hippocampus and amygdala both contain discrete but

317   spatially intermixed populations of neurons that code for fear and extinction (Lacagnina et al.,

318   2019; Senn et al., 2014; Zhang et al., 2020). Shifts in activity between these populations balances

319   the behavioral expression of emotional memories, in part through their differing long-range

320   connections with the mPFC (Marek et al., 2018; Senn et al., 2014; Sotres-Bayon et al., 2012).

321   Regions that exhibit bi-directional control over the expression of emotional memories could be

322   crucial for the proper regulation of fear and extinction in humans. Thus, on a trial-by-trial basis,

323   we assessed whether neural activity levels in the subfields of the hippocampus and amygdala

324   predicted the location of reinstatement between our two mPFC regions (vmPFC and dACC). We

325   restricted our analysis to CS items from conditioning and extinction as our time points of interest.

326   We found that all subfields were significant predictors of reinstatement location, such that

327   increases in MTL activity at the time of memory retrieval predicted more reinstatement in the

328   dACC (pHC: $X^2_{(1)} = 54.7$, P = 1.38e-13, slope = -1.8e-3; HC body: $X^2_{(1)} = 68.2$, P = 1.48e-16, slope

329   = -2.49e-3; aHC: $X^2_{(1)} = 46.8$, P = 8.00e-12, slope = -1.7e-3; BLA: $X^2_{(1)} = 26.7$, P = 2.39e-7, slope

330   = -1.45e-3; CeM: $X^2_{(1)} = 19.5$, P = 1.01e-5, slope = -6.90e-4). Additionally, we observed several

331   interactions with the hippocampal subfields, see **Supplementary Results**.

332   *MTL reinstatement.* Having established that overall activity in the MTL predicts more

333   reinstatement in the dACC, we next conducted a similar set of analyses in which trial-by-trial

334   reinstatement was used to predict the mPFC difference in reinstatement. The hypothesis for what

335 MTL reinstatement will predict is not automatically the same as what was observed for univariate

336 activity, as the information present in a spatial pattern of activity differs from the mean activity

337 across that pattern. Item-specific memory reinstatement in three subfields was predictive of

338 reinstatement in different regions of the mPFC (**Fig. 4**). Greater reinstatement in the pHC ($X^2_{(1)} =$

339 4.64, P = 0.031, slope = -0.060) and CeM ($X^2_{(1)} = 8.49$, P = 0.004, slope = -0.065) was associated

340 with a bias towards reinstatement in the dACC. In contrast, greater reinstatement in the aHC ($X^2_{(1)}$

341 = 11.1, P = 8.51e-4, slope = 0.091) was associated with a bias towards reinstatement in the

342 vmPFC. There were no significant interactions with encoding context, CS type, or group for any

343 of these subfields. Finally, reinstatement in the body of the hippocampus and the BLA did not

344 predict mPFC reinstatement location.

345
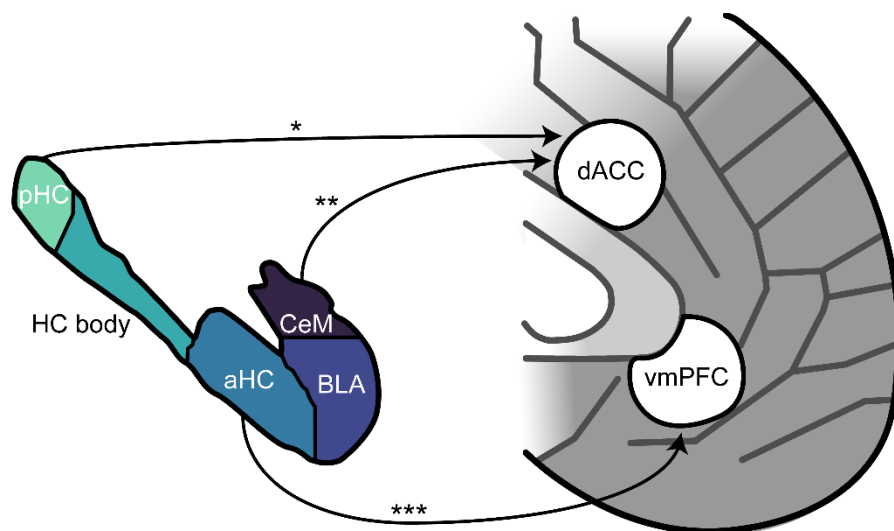
346 **Figure 4. MTL reinstatement predicts mPFC reinstatement location.** For each of the ROIs in
347 the hippocampus and amygdala, local reinstatement was used to predict the difference in
348 reinstatement in the mPFC. A stylized representation of the MTL and mPFC is shown. Arrows
349 indicate a significant prediction, the direction of which was determined by the slope; see text for
350 details. ***P < 0.001, **P < 0.01, *P < 0.05.

351

352 *Separable influence of the aHC.* We found that univariate and multivariate signals from

353 the aHC predict opposite biases in mPFC reinstatement during memory retrieval. Greater mean

354 activity in the aHC predicted a bias in reinstatement to the dACC, while greater reinstatement in

355   the same region predicted a bias to the vmPFC. Consistent with the proposition that the aHC

356   exerts bidirectional control over the expression of fear and extinction, we found that both neural

357   signatures were independently predictive of cortical reinstatement when combined into a single

358   model (univariate: $X^2_{(1)}$ = 42.5, P = 7.1e-11, slope = -1.65e-3; reinstatement: $X^2_{(1)}$ = 5.56, P =

359   0.018, slope = 0.067), with no significant interactions with either predictor.

Discussion

361   Extinction learning can build a memory of safety to countervail retrieval and expression of

362   the original fear association. However, an adaptive memory system should preserve the original

363   fear memory, as an experience of safety does not necessarily render a stimulus completely

364   harmless. These opposing associations should therefore be stored in a way that allows for the

365   appropriate behavior for a given context (Moorman and Aston-Jones, 2015). Neurobiological

366   research in rodents is beginning to reveal the structure of this organization within and between

367   discrete brain regions by quantifying the overlap in activity during memory formation and memory

368   expression (Letzkus et al., 2015; Reijmers et al., 2007; Tovote et al., 2015). Using multivoxel

369   pattern similarity analysis of overlapping encoding-to-retrieval activity in human neuroimaging, we

370   were able to identify a divided organization of fear and extinction memories in the mPFC and

371   hippocampus. Specifically, extinction memories were reinstated in the vmPFC and aHC, while

372   fear memories were reinstated in the dACC and pHC. Individuals with PTSS exhibited a similar

373   pattern of selective fear memory reinstatement. However, they surprisingly misallocated

374   extinction memories to regions selective for associative fear memory in healthy participants.

375   Across both groups, we observed that various neural signals from the MTL predicted the location

376   of cortical reinstatement of emotional memories in mPFC. These results bridge increasing

377   evidence from rodent neurophysiology for the divided organization of opposing associative

378   memories, and provide new insights into how disorganization in these neural representations may

379   contribute to psychiatric disease.

380   Previous findings from rodents show the PL is necessary for the long-term retrieval and

381   expression of conditioned fear (Corcoran and Quirk, 2007; Giustino and Maren, 2015). The PL

382   receives inputs from sensory cortices, the thalamus, and other PFC regions, in addition to

383   reciprocal connections with the amygdala and hippocampus (Hoover and Vertes, 2007). These

384   connections allow the PL to integrate information from the external environment as well as internal

385   states to flexibly guide behavior in potentially threatening situations. Here, we found that the dACC

386   reinstates activity patterns unique to the formation of associative fear memories, confirming a role

387   for this structure in the organization of long-term fear memories in the human brain. The dACC is

388   broadly activated by negative emotional stimuli (Etkin et al., 2011), including during emotional

389   episodic memory retrieval (Kensinger and Ford, 2021). A whole brain searchlight analysis also

390   revealed reinstatement of fear memories in the anterior insula, which together with the dACC are

391   hubs of the salience network (Seeley, 2019). Collectively, fear memory representations appear

392   distributed across cortical and subcortical networks that may code for unique aspects of the fear

393   experience (Frankland et al., 2019; Wheeler et al., 2013). Orchestration between these regions

394   likely determines retrieval of fear memory over extinction memory.

395   The rodent IL is necessary for the long-term retention of extinction memories (Do-Monte

396   et al., 2015), and is inhibited by the ventral hippocampus during fear renewal (Marek et al., 2018).

397   Here, we found that the vmPFC reinstates activity patterns unique to the formation of an extinction

398   memory in the healthy adult brain. Notably, univariate human neuroimaging evidence for the

399   involvement of the vmPFC in extinction learning and recall has been limited and mixed (Fullana

400   et al., 2018). The present finding thus helps bridge extensive evidence from rodents to humans

401   on the role of this region in organizing extinction memory to inhibit retrieval and expression of fear

402   associations. We also found that individuals with PTSD symptoms displayed an abnormal

403   organization of fear and extinction reinstatement in the mPFC. Specifically, the dACC exhibited

404   reinstatement of memories formed during extinction, while there was an absence of selective

405   extinction memory reinstatement in the vmPFC. Critically, behavioral performance of within-

406   session extinction learning was not different between groups, and both groups remembered an

407   equivalent number of items encoded during extinction. Thus, distinctions in neural reinstatement

408   of extinction memory appear to reflect an underlying distinction in how an implicit extinction

409   memory trace is formed and retrieved; they do not merely recapitulate an observable behavioral

410   deficit. This suggests that individuals with a history of trauma may utilize a different, and ultimately

411   maladaptive, neural mechanism for fear reduction during within-session extinction learning that

412   bypasses the formation of a long-term extinction memory trace in the vmPFC. Interestingly,

413   evidence from rodent studies shows the IL is not necessarily required for within-session extinction,

414   only for successful extinction retrieval (Do-Monte et al., 2015). However stimulation of the vmPFC

415   during or after extinction learning improves extinction retention (Do-Monte et al., 2015; Dunsmoor

416   et al., 2019; Haaker et al., 2013; Milad et al., 2004; Raij et al., 2018). The inability to form an initial

417   memory trace of extinction learning in the vmPFC, to be retrieved at a later time, may therefore

418   be a critical factor in extinction retrieval deficits observed in PTSD (Lissek and van Meurs, 2015;

419   Pitman et al., 2012). Likewise, the misallocation of extinction-specific memories to the dACC,

420   rather than the vmPFC, may bias the retrieval and expression of fear associations following

421   extinction, further contributing to fear relapse. These provide potential targets to strengthen

422   extinction memory for clinical purposes.

423   We also found divided organization of fear and extinction memories along the long axis of

424   the hippocampus. Interestingly, neural reinstatement in the hippocampus was sensitive to the

425   temporal context of encoding (fear versus extinction) rather than the valence of the CS (CS+

426   versus CS-). This division of contextual specificity aligns with the general role of the hippocampus

427   in forming contextual representation in associative learning (O'Reilly and Rudy, 2001) and

428   exerting contextual control of extinction retrieval through connections with the mPFC (Bouton et

429   al., 2020; Marek et al., 2018). The hippocampus maintains competing representations of fear and

430   extinction memory in distinct neural populations in the dentate gyrus (Lacagnina et al., 2019) and

431   CA1 (Tronson et al., 2009). Whether there is a division in dorsal and ventral regions in the

432   representation of fear versus extinction memory is less clear. This organization is likely

433   determined by dissociable connectivity with subregions of the mPFC (Bast et al., 2003; Corcoran

434   et al., 2005; Marek et al., 2018; Meyer et al., 2019; Qin et al., 2021; Sierra-Mercado et al., 2011;

435   Twining et al., 2020; Ye et al., 2017). Our results suggest that the pHC is involved in the retrieval

436   of fear memories, as both healthy adults and those with PTSS displayed selective reinstatement

437   in the pHC for items encoded during fear conditioning. Additionally, neural reinstatement in the

438   pHC, as well as univariate activity at the time of retrieval, predicted a bias in mPFC reinstatement

439   towards the dACC. The aHC, in contrast, showed selective reinstatement for items encoded in

440   the extinction context. However, further analysis showed that the aHC serves a dual role in

441   retrieval of fear and extinction memory. On one hand, neural reinstatement in the aHC predicted

442   neural reinstatement in the vmPFC, suggesting a network for extinction memory organization. On

443   the other hand, univariate activity in the aHC at the time of memory retrieval predicted

444   reinstatement in the dACC, consistent with a separate network that may facilitate retrieval of

445   associative fear memories. The aHC therefore appears well situated for integrating contextual

446   information and gating retrieval of the fear or extinction memory through connections with the

447   dACC or vmPFC, respectively.

448   Given considerable evidence of reactivation of fear engrams in the rodent basolateral

449   amygdala (e.g., (Reijmers et al., 2007)), it is notable that we did not observe reinstatement in the

450   human amygdala. One possibility is that participants were not under threat at retrieval, thereby

451   limiting involvement of the amygdala for behavioral fear expression. However, there was a general

452   lack of amygdala involvement at encoding as well, consistent with meta-analyses of fMRI of

453   human fear conditioning (Fullana et al., 2016, 2018, 2019). The spatial resolution limitations of

454   fMRI are perhaps unable to separate reactivation of sparse neural population coding for both fear

455 and extinction memories (Herry et al., 2010), as well as the CS+ and CS- (Ghosh and Chattarji,

456 2015). Although we did not observe selective reinstatement in the amygdala, univariate activity in

457 the amygdala during retrieval, as well as local reinstatement in the CeM, predicted reinstatement

458 in the dACC over the vmPFC (**Fig. 4**). This is consistent with the idea that reciprocal connections

459 between the amygdala and mPFC organizes the storage and retrieval of fear memories (Tovote

460 et al., 2015).

461   To conclude, much of the progress in the past decade on the neuroscience of fear and

462 extinction has utilized activity-dependent functional labeling to identify the neural organization of

463 these opposing memories (Frankland et al., 2019; Tovote et al., 2015). Here we provide evidence

464 for selective neural reinstatement of fear and extinction memory representations in the human

465 brain through overlapping activity patterns at encoding and retrieval. These results extend a

466 conceptual framework of engram-like representations, and more broadly bolsters the use of

467 multivariate pattern analyses to translate cutting-edge advances in the neurobiology of fear and

468 extinction to humans (Bach et al., 2011; Graner et al., 2020; Hennings et al., 2020; Visser et al.,

469 2013). The hybrid episodic/conditioning design incorporated here afforded us simultaneous

470 access to isolate memories that normally exert reciprocal inhibition during a traditional test of an

471 extinguished memory (e.g., spontaneous recovery or renewal test). Selective neural

472 reinstatement of competing memories formed under different temporal contexts is predicted by

473 the encoding-specificity principle (Tulving and Thomson, 1973) and neural reinstatement of

474 episodic memory in human neuroimaging (Polyn et al., 2005; Ritchey et al., 2013), but has not

475 previously been shown for fear and extinction memory in humans. This design may be applied to

476 future work in humans seeking to assess the efficacy of protocols that enhance extinction

477 (Dunsmoor et al., 2015b) or modify the underlying fear memory trace through reconsolidation

478 updating (Ressler et al., 2021). A further possibility to extend this work is to target engagement of

479 activity patterns unique to formation of an extinction memory in distributed networks through

480 closed-loop decoded neurofeedback (Taschereau-Dumouchel et al., 2018, 2020) to create an

481 enduring memory of safety. In this way, more precise localization of networks involved in

482 organizing fear and extinction memory could ultimately lead to better treatments of psychiatric

483 disorders like PTSD.

484 **ONLINE METHODS**

485 **Participants**.

486 A total of 48 participants from the community volunteered to complete the two-day

487 functional MRI study. Three additional participants were recruited but did not complete the

488 experiment. Half of the participants (N = 24; 15 female; Mean age = 21) were recruited with the

489 criteria that they have no current or past psychiatric or neurological disorders. The remaining

490 participants (N = 24; 17 female; Mean age = 26) were recruited after responding to flyers seeking

491 volunteers with PTSD. These participants underwent phone screening and completed additional

492 in-person questionnaires to confirm Criterion A trauma exposure on the PTSD checklist for DSM-

493 5 (PCL) (Blevins et al., 2015), as well as the absence of other neurological disorders. All PTSD

494 responding participants reported significant post-trauma symptoms related to a Criterion A

495 trauma, however we refer to this cohort as having post-traumatic stress symptoms (PTSS) as we

496 did not implement a structured diagnostic interview. Given high rates of co-morbid substance use

497 disorder, all PTSS participants were given a urine toxicology screening, and no participants tested

498 positive for illicit drugs or benzodiazepines. Written informed consent was obtained for all

499 participants, and all experimental procedures were approved by the University of Texas at Austin

500 IRB (#2017-02-0094). PCL scores, as well as surveys of anxiety and depression are reported in

501 Hennings et al., 2020.

502 **Stimuli.**

503 Conditioned stimuli were images of animals and tools collected from lifeonwhite.com or

504 other publicly available resources on the internet. Critical to the design of the task, each stimulus

505   was a unique exemplar from its category. For example, there were not two different kinds of "dog"

506   used. Typically phobic animals or threatening tools were excluded (e.g., spiders, snakes, knives).

507   The unconditioned stimulus (US) was a brief (50ms) electric shock delivered to fingers of the left

508   hand. Prior to entering the scanner, the US was calibrated for each participant to a level described

509   as "highly annoying and unpleasant, but not painful". A BIOPAC STMEPM-MRI module was used

510   to deliver the US (Goleta, CA). During the recognition memory test, all 144 "old" stimuli were

511   shown, in addition to 48 novel lures per category. CSs were presented for 3s followed by a 4 or

512   5s ITI (jittered). Trial order was again pseudorandomized to ensure a balance of CSs from each

513   encoding phase as well as old and new items. Stimulus presentation was controlled using E-

514   Prime 3.0.

515   **Task.**

516   *Associative learning task*. Participants completed an associative learning task in two

517   sessions of about an hour each, roughly 24 hours apart. We note that "fear" can be a misnomer

518   of the emotional construct being studied in research involving human participants (LeDoux and

519   Pine, 2016). A better term may be "threat conditioning"*,* as it better captures both the actual

520   emotional experience of participants and the acquisition of conditioned responses. Nevertheless,

521   we retain the term "fear*"* to connect the results the broader field of Pavlovian conditioning across

522   model organisms. For all phases of the associative learning task, images were displayed for 4.5

523   +/- 0.5s (jittered), and the ITI between trials lasted 6 +/- 0.5s (jittered). The trial order of the CSs

524   was pseudorandomized to ensure no more than 3 CS type were presented in a row. The same

525   pseudorandomized order was used for all subjects, however which phase of the experiment each

526   stimulus was displayed was randomized across participants. Day 1 consisted of pre-conditioning,

527   fear conditioning, and extinction. On Day 1, each phase consisted of 48 trials, 24 animals and 24

528   tools, for a total of 144 items. During pre-conditioning, participants identified which category each

529   image belonged to (2-alternative forced choice, 2-AFC; animal or tool). During fear conditioning,

530   50% of the trials from one category (CS+) co-terminated with the US, for a total of 12 CS+US

531 pairings. Images from the other category were never paired with shock (CS-), and the category

532 of the CS+ was counterbalanced across participants. Extinction learning followed fear

533 conditioning, during which no shocks were delivered. Relevant to hypotheses explained in

534 Hennings et al., 2020, during extinction learning the normal fixation cross displayed during the ITI

535 was replaced with a stream of natural scene images displayed for 1s each (5, 6, or 7 scenes per

536 ITI). During fear conditioning and extinction on Day 1, participants responded whether or not they

537 expected a shock on each trial (2-AFC; yes or no). Skin-conductance responses were collected

538 during pre-conditioning, fear condition, and extinction. The following day, participants had the

539 electrodes reattached prior to entering the scanner for the fear renewal test (reported in Hennings

540 et al., 2020).

541 *Recognition memory test*. After completing the fear renewal test on Day 2, participants

542 completed a surprise recognition memory test for the items they had seen the previous day.

543 Participants were informed that no shocks would be delivered during the memory test. All 144 old

544 images were included as well as 96 novel foils. The stimuli seen during the fear renewal test were

545 not shown during the recognition memory test. Each image was displayed for 3s with a 4 or 5s

546 ITI, and participants indicated whether each image was old (they had seen it the previous day),

547 or new (never seen before). Participants indicated the confidence of their choice by responding

548 the image was definitely old, maybe old, maybe new, or definitely new. The memory test was split

549 into three fMRI runs of equal length, and trial order was again pseudorandomized to ensure a

550 balance of lures and foils of both CS types and encoding phases across the memory runs. Trials

551 during the recognition memory test were removed from analysis if participants failed to make a

552 response within the 3s window (Mean = 2.5 dropped "old" trials per participant). A perceptual

553 localizer followed the recognition memory test to facilitate MVPA decoding, however this data was

554 not used in the present analyses.

555 **Functional MRI acquisition.**

556   Neuroimaging was accomplished using the Siemens Skyra 3T Human MRI scanner

557   located at the Biomedical Imaging Center at the University of Texas at Austin. Functional data

558   were acquired with a 32-channel head-coil, with 3mm isotropic resolution (TR = 2000ms; TE =

559   29ms; FoV = 228; 48 slices). A multi-band factor of 2 was used with automatic AC/PC alignment.

560   As discussed in Hennings et al., (2020), due to a computer malfunction, 2 subjects had slightly

561   different acquisition parameters on Day 1 (TR = 2230ms; 66 slices), which were accounted for

562   during preprocessing and analysis. An T1-weighted 3d MPRAGE scan (TR = 1900ms; 1mm

563   isotropic resolution) was collected on Day 1 to aid in functional image registration and region of

564   interest definition.

565   **Image preprocessing**

566   Functional MRI data were processed using *fMRIprep* (v1.5.4)*,* an open source software

567   suite designed to increase reproducibility and develop common best practices for image

568   processing. The following boilerplate has been included unchanged, as recommended by the

569   package maintainers.

570   *Anatomical data preprocessnoning.* The T1-weighted (T1w) image was corrected for

571   intensity non-uniformity (INU) with N4BiasFieldCorrection (Tustison et al., 2010), distributed

572   with ANTs 2.2.0 (Avants et al., 2008), and used as T1w-reference throughout the workflow. The

573   T1w-reference   was   then   skull-stripped   with   a *Nipype* implementation   of

574   the antsBrainExtraction.sh workflow (from ANTs), using OASIS30ANTs as target

575   template. Brain tissue segmentation of cerebrospinal fluid (CSF), white-matter (WM) and gray-

576   matter (GM) was performed on the brain-extracted T1w using fast (FSL 5.0.9 (Zhang et al.,

577   2001)). Brain surfaces were reconstructed using recon-all (FreeSurfer 6.0.1, (Dale et al., 1999)),

578   and the brain mask estimated previously was refined with a custom variation of the method to

579   reconcile ANTs-derived and FreeSurfer-derived segmentations of the cortical gray-matter of

580   Mindboggle (Klein et al., 2017). Volume-based spatial normalization to one standard space

581   (MNI152NLin2009cAsym) was performed through nonlinear registration

582   with `antsRegistration` (ANTs 2.2.0), using brain-extracted versions of both T1w reference

583   and the T1w template. The following template was selected for spatial normalization: *ICBM 152*

584   *Nonlinear Asymmetrical template version 2009c* (Fonov et al., 2009).

585   *Functional data preprocessing.* For each of the 9 BOLD runs found per subject (across all

586   tasks and sessions), the following preprocessing was performed. First, a reference volume and

587   its skull-stripped version were generated using a custom methodology of *fMRIPrep*. Susceptibility

588   distortion correction (SDC) was omitted as no field maps were collected. The BOLD reference

589   was then co-registered to the T1w reference using `bbregister` (FreeSurfer) which implements

590   boundary-based registration (Greve and Fischl, 2009). Co-registration was configured with six

591   degrees of freedom. Head-motion parameters with respect to the BOLD reference (transformation

592   matrices, and six corresponding rotation and translation parameters) are estimated before any

593   spatiotemporal filtering using `mcflirt` (FSL 5.0.9 (Jenkinson et al., 2002)). BOLD runs were

594   slice-time corrected using `3dTshift` from AFNI 20160207 (Cox and Hyde, 1997). The BOLD

595   time-series (including slice-timing correction when applied) were resampled onto their original,

596   native space by applying the transforms to correct for head-motion. These resampled BOLD time-

597   series will be referred to as *preprocessed BOLD in original space*, or just *preprocessed BOLD*.

598   The BOLD time-series were resampled into standard space, generating a *preprocessed BOLD*

599   *run in MNI152NLin2009cAsym space*. First, a reference volume and its skull-stripped version

600   were generated using a custom methodology of *fMRIPrep*. Several confounding time-series were

601   calculated based on the *preprocessed BOLD*: framewise displacement (FD), DVARS and three

602   region-wise global signals. FD and DVARS are calculated for each functional run, both using their

603   implementations in *Nipype* (following the definitions by (Power et al., 2014)). The three global

604   signals are extracted within the CSF, the WM, and the whole-brain masks. Additionally, a set of

605   physiological regressors were extracted to allow for component-based noise

606   correction (*CompCor* (Behzadi et al., 2007)). Principal components are estimated after high-pass

607   filtering the *preprocessed BOLD* time-series (using a discrete cosine filter with 128s cut-off) for

608   the two *CompCor* variants: temporal (tCompCor) and anatomical (aCompCor). tCompCor

609   components are then calculated from the top 5% variable voxels within a mask covering the

610   subcortical regions. This subcortical mask is obtained by heavily eroding the brain mask, which

611   ensures it does not include cortical GM regions. For aCompCor, components are calculated within

612   the intersection of the aforementioned mask and the union of CSF and WM masks calculated in

613   T1w space, after their projection to the native space of each functional run (using the inverse

614   BOLD-to-T1w transformation). Components are also calculated separately within the WM and

615   CSF masks. For each CompCor decomposition, the *k* components with the largest singular

616   values are retained, such that the retained components' time series are sufficient to explain 50

617   percent of variance across the nuisance mask (CSF, WM, combined, or temporal). The remaining

618   components are dropped from consideration. The head-motion estimates calculated in the

619   correction step were also placed within the corresponding confounds file. The confound time

620   series derived from head motion estimates and global signals were expanded with the inclusion

621   of temporal derivatives and quadratic terms for each (Satterthwaite et al., 2013). Frames that

622   exceeded a threshold of 0.5 mm FD or 1.5 standardized DVARS were annotated as motion

623   outliers. All resamplings can be performed with *a single interpolation step* by composing all the

624   pertinent transformations (i.e. head-motion transform matrices, susceptibility distortion correction

625   when available, and co-registrations to anatomical and output spaces). Gridded (volumetric)

626   resamplings were performed using `antsApplyTransforms` (ANTs), configured with Lanczos

627   interpolation to minimize the smoothing effects of other kernels (Lanczos, 1964). Non-gridded

628   (surface) resamplings were performed using `mri_vol2surf` (FreeSurfer).

629   **Region of interest selection**

630   The dACC, vmPFC, hippocampus, and amygdala were selected *a priori* to test for the

631   presence of encoding specificity of fear and extinction memories. Prefrontal ROIs were based on

632   peak coordinates previously reported in literature. Specifically, dACC coordinates (MNI 1, 21, 27)

633   were taken from (Milad et al., 2007) in which a univariate contrast of CS+ > CS- during fear

634   conditioning was used. vmPFC coordinates (MNI -4, 34, -6) were taken from an fMRI meta-

635   analysis of extinction recall (Fullana et al., 2018), using a univariate contrast of CS+ extinguished

636   > CS+ unextinguished. For each ROI, a sphere was drawn around the coordinates with a radius

637   of 10mm, and was then restricted to grey matter using a grey matter probability mask with a

638   threshold of 50%. The masks were then warped to subject space to achieve native functional

639   resolution (3mm^3) for multivariate analyses. Registration was accomplished using `flirt` using

640   12 degrees of freedom and nearest neighbor interpolation for each binary mask (FSL 5.0.9

641   (Jenkinson et al., 2012)).

642   The hippocampus and amygdala were masked and segmented into subfields using

643   Freesurfer's `segmentHA_T1` on the preprocessed T1w anatomical images from `recon-all`

644   (Freesurfer 7.0 (Fischl, 2012; Iglesias et al., 2015; Saygin et al., 2017)). The hippocampus was

645   segmented into head (anterior), body, and tail (posterior) subfields along the long axis. The

646   amygdala was segmented into the basolateral (BLA), and central nucleus (CeM) subfields. The

647   anatomical segmentations were registered to functional space using `mri_label2vol` and binary

648   masks created using `fslmaths`.

Multivariate pattern analysis

650   After preprocessing with fMRIprep, we computed a LS-S style betaseries to facilitate the

651   encoding-retrieval similarity analysis (Mumford et al., 2012, 2014). For each scanner run, trial-

652   specific beta images are computed iteratively using a general linear model (GLM) which models

653   a single trial of interest and all other trials as regressors of no interest based on trial type (separate

654   CS+/- no interest regressors). In addition to the betaseries images, we also generated

655   conventional average activity estimates for CS+ and CS- separately from each phase of learning

656   on Day 1, (i.e., all CS+ in one regressor of interest). For GLMs of fear conditioning, the US was

657   modeled as a 0 duration event and treated as a regressor of no interest. All GLM estimation was

658   accomplished using FSL `FEAT,` prewhitening was used, and spatial smoothing was not applied

659   in order to respect the boundaries of our *a priori* ROIs. In addition to the preprocessing applied

660   by fMRIprep, several signals were included as confounds to be removed during GLM estimation,

661   including the first principle component of the estimated physiological noise (aCompCor),

662   framewise displacement, 6 standard motion parameters, and the discrete cosine-basis regressors

663   calculated by fMRIprep for high-pass filtering.

664   The encoding-retrieval similarity analysis was implemented in custom Python code. The

665   goal of this analysis was to directly compare multi-voxel patterns observed during encoding and

666   retrieval of a specific stimulus in each ROI on a per-participant basis. In order to reduce noise

667   prior to estimating pattern similarity, the LS-S beta images were weighted (multiplied) by the

668   overall univariate estimate of the corresponding CS type from encoding (Hennings et al., 2020;

669   Kim et al., 2020) (e.g. all images of extinction CS+s from encoding and retrieval were weighted

670   by the univariate estimate of extinction CS+ activity during encoding). For each ROI, encoding-

671   retrieval similarity was then taken as the Pearson's correlation between the two beta images for

672   a given stimulus, one from encoding and one from retrieval. Pearson's r values were Fisher-z

673   transformed and submitted to statistical analysis.

674   **Whole-brain searchlight.**

675   The searchlight analysis (Etzel et al., 2013; Kriegeskorte et al., 2006) was accomplished

676   using the *nilearn* package in Python using the functional resolution images ($3mm^3$) registered to

677   MNI space. Images were prepared as described above, and then each pair of beta images from

678   encoding and retrieval was submitted to a whole-brain searchlight analysis in which a Pearson's

679   correlation was iteratively computed in every sphere (radius = 6mm) in the brain. The resulting

680   maps were Fisher-z transformed, and averaged by CS type and encoding context for each

681   subject. For each encoding context, the difference between the average CS+ – CS- maps was

682   taken and analyzed using AFNI (v20.2.18) (Cox, 1996; Cox and Hyde, 1997; Gold et al., 1998).

683   Specifically, `3dttest++` was used to test the CS+ – CS- difference against 0 for each encoding

684   context and for each group. The analysis was restricted to voxels that had ≥ 50% grey matter

685   probability. Family-wise error correction was achieved using the `-Clustsim` option, which uses

686   permutation testing to simulate the null distribution of the data in order to determine the threshold

687   necessary to observe significant clusters. Clusters were extracted using `3dClusterize` using a

688   peak threshold of P < 0.001 (one-tailed CS+ – CS-), and a cluster threshold corresponding to P

689   < 0.05 using full voxel connectivity. The size of the cluster necessary to reach this threshold

690   ranged from 16-21 across the 4 maps. The coordinates of the peak voxel in each cluster were

691   submitted to the AFNI function `whereami` to obtain anatomical labels based on the Talairach-

692   Tournoux Atlas (Talairach, 1988). The *pysurfer* package in Python was used to resample and

693   slightly smooth (FWHM = 1mm) the cluster maps onto the cortical surface for display purposes.

694   **Statistical analyses.**

695   With the exception of the whole-brain searchlight analysis (see above), all statistical tests

696   are reported as two-tailed, and all estimates of error are given as parametric 95% confidence

697   intervals (i.e., 1.96 * standard error of the mean). Behavioral data was analyzed using the *pingouin*

698   (Vallat, 2018) package in Python and the *ez* (Lawrence, 2016) package in R. As discussed in

699   Hennings et al., (2020) due to technical errors four participants (two in each group) are missing

700   SCR data from extinction. SCR was square-root transformed prior to analysis and analyzed using

701   paired and independent samples t-tests (see Hennings et al., 2020 for description of SCR scoring

702   method). 2-AFC shock expectancy from conditioning and extinction was coded as 1 = expect, and

703   0 = do not expect, and analyzed using paired and independent samples t-tests. As our neural

704   analysis focused on the reinstatement of previously encoded items, the analysis of recognition

705   memory focused on high confidence hits (i.e. definitely old responses). Hit rates were submitted

706   to a mixed ANOVA with within subject factors of *encoding context* and *CS type*, and a between

707   subjects factor of *group*

708   All other statistical analyses were accomplished with linear mixed effects models using

709   the *afex* (Singmann et al., 2015) package in R with maximum likelihood estimation. Encoding-

710   retrieval similarity was analyzed on a trial wise basis, and the model included fixed effects of CS

711   type, encoding context, subfield, and group, as well as a random intercept of subject

712   (*reinstatement ~ CS type * encoding context * subfield * group* + (1|*subject*)). The subfield term

713   here represents the vmPFC/dACC when modeling reinstatement in the mPFC, and the

714   subdivisions of the hippocampus and amygdala for reinstatement in those structures. Significance

715   of the main effects and interactions of the fixed effects was evaluated using Chi-square tests,

716   comparing the log-likelihoods of a model with and without the term of interest (Luke, 2017). All

717   possible interactions were modeled, and the highest order interaction is reported for a given effect

718   when relevant. When testing the double dissociations of reinstatement in the mPFC and

719   hippocampus, data was restricted to CS items from conditioning and extinction, and a separate

720   model was fit for each group (without the *group* term). All Planned and *post-hoc* contrasts were

721   accomplished using the *emmeans* (Lenth, 2019) package in R. Asymptotic degrees of freedom

722   were used, as in general the number of observations in each model was quite large (between

723   ~4,000 up to ~20,000). Parametric 95% confidence intervals of the differences are reported along

724   with FDR corrected P-values using the `p.adjust` function in R. FDR correction was applied to

725   each family of tests in each group of ROIs; for example, FDR correction was applied to the 12

726   tests of CS+ – CS- reinstatement in the mPFC (2 ROIs, 3 contexts, 2 groups). FDR correction

727   was also applied at the next level of analysis; for example, the 4 cross-ROI comparisons of CS+

728   – CS- reinstatement in the mPFC (2 ROIs, 2 groups).

729   Linear mixed-effects models were also used to evaluate whether MTL activity predicted

730   the difference in mPFC reinstatement (*vmPFC – dACC reinstatement ~ predictor * CS type **

731   *encoding context * group* + (1|*subject*)). In all cases our analysis focused only on the main effect

732   and interactions of *predictor,* which was iteratively univariate activity or local reinstatement from

733   all MTL ROIs. The same procedure was used to evaluate the separable contributions of univariate

734   activity and reinstatement in the aHC; both neural signals were entered as predictors in a single

735   model. Significance of main effects and interactions was again determined using log-likelihood

736   ratio tests and point estimates and parametric 95% confidence intervals of the slopes were

737   obtained using the `emtrends` function from *emmeans*.

738 **AUTHOR CONTRIBUTIONS**

739   A.C.H., J.E.D, and J. A. L.P., conceived of and designed the fMRI experiment. A.C.H. and M. M.

740   implemented the fMRI experiment and collected the data. A.C.H preprocessed and analyzed the

741   data and visualized results. A.C.H, J.E.D., and J.A.L.P. wrote the original draft of the manuscript.

742   A.C.H, M.R.D., J.E.D., and J.A.L.P. reviewed and edited the final draft of the manuscript.

743 **COMPETING INTEREST STATEMENT**

744   The authors declare that they have no competing interests.

745 **DATA AVAILABILITY STATEMENT**

746   All deidentified neuroimaging and behavioral data may be found online at https://osf.io/qeg83/

747 **CODE AVAILABILITY STATEMENT**

748   All custom python and R code used for analysis will be made available at https://osf.io/qeg83/

749 **REFERENCES**

750 Avants, B.B., Epstein, C.L., Grossman, M., and Gee, J.C. (2008). Symmetric diffeomorphic
751   image registration with cross-correlation: Evaluating automated labeling of elderly and
752   neurodegenerative brain. Medical Image Analysis *12*, 26–41.

753 Bach, D.R., Weiskopf, N., and Dolan, R.J. (2011). A stable sparse fear memory trace in human
754   amygdala. Journal of Neuroscience *31*, 9383–9389.

755 Bast, T., Zhang, W.N., and Feldon, J. (2003). Dorsal hippocampus and classical fear
756   conditioning to tone and context in rats: Effects of local NMDA-receptor blockade and
757   stimulation. Hippocampus *13*, 657–675.

758 Behzadi, Y., Restom, K., Liau, J., and Liu, T.T. (2007). A component based noise correction
759   method (CompCor) for BOLD and perfusion based fMRI. NeuroImage *37*, 90–101.

760 Blevins, C.A., Weathers, F.W., Davis, M.T., Witte, T.K., and Domino, J.L. (2015). The
761   Posttraumatic Stress Disorder Checklist for DSM-5 (PCL-5): Development and Initial
762   Psychometric Evaluation. Journal of Traumatic Stress *28*, 489–498.

763 Bouton, M.E., Maren, S., and McNally, G.P. (2020). Behavioral and neurobiological mechanisms
764   of pavlovian and instrumental extinction learning. Physiological Reviews *101*, 611–681.

765 Burgos-Robles, A., Vidal-Gonzalez, I., and Quirk, G.J. (2009). Sustained conditioned responses
766   in prelimbic prefrontal neurons are correlated with fear expression and extinction failure.
767   Journal of Neuroscience *29*, 8474–8482.

768 Burgos-Robles, A., Kimchi, E.Y., Izadmehr, E.M., Porzenheim, M.J., Ramos-Guasp, W.A., Nieh,
769   E.H., Felix-Ortiz, A.C., Namburi, P., Leppla, C.A., Presbrey, K.N., et al. (2017). Amygdala
770   inputs to prefrontal cortex guide behavior amid conflicting cues of reward and punishment.
771   Nature Neuroscience *20*, 824–835.

772 Cooper, R.A., and Ritchey, M. (2019). Cortico-hippocampal network connections support the
773   multidimensional quality of episodic memory. ELife *8*.

774 Corcoran, K.A., and Quirk, G.J. (2007). Activity in Prelimbic Cortex Is Necessary for the
775   Expression of Learned, But Not Innate, Fears. Journal of Neuroscience *27*, 840–844.

776 Corcoran, K.A., Desmond, T.J., Frey, K.A., and Maren, S. (2005). Hippocampal inactivation
777   disrupts the acquisition and contextual encoding of fear extinction. Journal of
778   Neuroscience *25*, 8978–8987.

779 Cox, R.W. (1996). AFNI: software for analysis and visualization of functional magnetic resonance
780   neuroimages. Comput Biomed Res *29*, 162–173.

781 Cox, R.W., and Hyde, J.S. (1997). Software tools for analysis and visualization of fMRI data.
782   NMR Biomed *10*, 171–178.

783 Dale, A.M., Fischl, B., and Sereno, M.I. (1999). Cortical surface-based analysis: I. Segmentation
784   and surface reconstruction. NeuroImage *9*, 179–194.

785 Davis, P., Zaki, Y., Maguire, J., and Reijmers, L.G. (2017). Cellular and oscillatory substrates of
786   fear extinction learning. Nat Neurosci *20*, 1624–1633.

787 Do-Monte, F.H., Manzano-Nieves, G., Quiñones-Laracuente, K., Ramos-Medina, L., and Quirk,
788   G.J. (2015). Revisiting the role of infralimbic cortex in fear extinction with optogenetics.
789   Journal of Neuroscience *35*, 3607–3615.

790 Dunsmoor, J.E., and Kroes, M.C. (2019). Episodic memory and Pavlovian conditioning: ships
791   passing in the night. Current Opinion in Behavioral Sciences *26*, 32–39.

Dunsmoor, J.E., Murty, V.P., Davachi, L., and Phelps, E.A. (2015a). Emotional learning
    selectively and retroactively strengthens memories for related events. Nature *520*, 345–
    348.

Dunsmoor, J.E., Niv, Y., Daw, N., and Phelps, E.A. (2015b). Rethinking Extinction. Neuron *88*,
    47–63.

Dunsmoor, J.E., Kroes, M.C.W., Moscatelli, C.M., Evans, M.D., Davachi, L., and Phelps, E.A.
    (2018). Event segmentation protects emotional memories from competing experiences
    encoded close in time. Nature Human Behaviour *2*, 291–299.

Dunsmoor, J.E., Kroes, M.C.W., Li, J., Daw, N.D., Simpson, H.B., and Phelps, E.A. (2019). Role
    of human ventromedial prefrontal cortex in learning and recall of enhanced extinction. The
    Journal of Neuroscience 2713–2718.

Etkin, A., Egner, T., and Kalisch, R. (2011). Emotional processing in anterior cingulate and
    medial prefrontal cortex. Trends in Cognitive Sciences *15*, 85–93.

Etzel, J.A., Zacks, J.M., and Braver, T.S. (2013). Searchlight analysis: Promise, pitfalls, and
    potential. NeuroImage *78*, 261–269.

Fischl, B. (2012). FreeSurfer. NeuroImage *62*, 774–781.

Fonov, V., Evans, A., McKinstry, R., Almli, C., and Collins, D. (2009). Unbiased nonlinear
    average age-appropriate brain templates from birth to adulthood. NeuroImage *47*, S102.

Frankland, P.W., Josselyn, S.A., and Köhler, S. (2019). The neurobiological foundation of
    memory retrieval. Nature Neuroscience *22*, 1576–1585.

Fullana, M.A., Harrison, B.J., Soriano-Mas, C., Vervliet, B., Cardoner, N., Àvila-Parcet, A., and
    Radua, J. (2016). Neural signatures of human fear conditioning: An updated and extended
    meta-analysis of fMRI studies. Molecular Psychiatry *21*, 500–508.

Fullana, M.A., Albajes-Eizagirre, A., Soriano-Mas, C., Vervliet, B., Cardoner, N., Benet, O.,
    Radua, J., and Harrison, B.J. (2018). Fear extinction in the human brain: a meta-analysis
    of fMRI studies in healthy participants. Neuroscience & Biobehavioral Reviews *88*, 16–25.

Fullana, M.A., Albajes-Eizagirre, A., Soriano-Mas, C., Vervliet, B., Cardoner, N., Benet, O.,
    Radua, J., and Harrison, B.J. (2019). Amygdala where art thou? Neuroscience and
    Biobehavioral Reviews *102*, 430–431.

Ghosh, S., and Chattarji, S. (2015). Neuronal encoding of the switch from specific to generalized
    fear. Nature Neuroscience *18*, 112–120.

Giustino, T.F., and Maren, S. (2015). The Role of the Medial Prefrontal Cortex in the
    Conditioning and Extinction of Fear. Front. Behav. Neurosci. *9*.

Gold, S., Christian, B., Arndt, S., Zeien, G., Cizadlo, T., Johnson, D.L., Flaum, M., and
    Andreasen, N.C. (1998). Functional MRI statistical software packages: a comparative
    analysis. Hum Brain Mapp *6*, 73–84.

828 Graner, J.L., Stjepanović, D., and LaBar, K.S. (2020). Extinction learning alters the neural
829   representation of conditioned fear. Cognitive, Affective and Behavioral Neuroscience.

830 Greve, D.N., and Fischl, B. (2009). Accurate and robust brain image alignment using boundary-
831   based registration. NeuroImage *48*, 63–72.

832 Haaker, J., Gaburro, S., Sah, A., Gartmann, N., Lonsdorf, T.B., Meier, K., Singewald, N., Pape,
833   H.-C., Morellini, F., and Kalisch, R. (2013). Single dose of L-dopa makes extinction
834   memories context-independent and prevents the return of fear. Proceedings of the
835   National Academy of Sciences *110*, E2428–E2436.

836 Hennings, A.C., McClay, M., Lewis-Peacock, J.A., and Dunsmoor, J.E. (2020). Contextual
837   reinstatement promotes extinction generalization in healthy adults but not PTSD.
838   Neuropsychologia *147*, 107573.

839 Herry, C., Ciocchi, S., Senn, V., Demmou, L., Müller, C., and Lüthi, A. (2008). Switching on and
840   off fear by distinct neuronal circuits. Nature *454*, 600–606.

841 Herry, C., Ferraguti, F., Singewald, N., Letzkus, J.J., Ehrlich, I., and Lüthi, A. (2010). Neuronal
842   circuits of fear extinction. European Journal of Neuroscience *31*, 599–612.

843 Hoover, W.B., and Vertes, R.P. (2007). Anatomical analysis of afferent projections to the medial
844   prefrontal cortex in the rat. Brain Struct Funct *212*, 149–179.

845 Iglesias, J.E., Augustinack, J.C., Nguyen, K., Player, C.M., Player, A., Wright, M., Roy, N.,
846   Frosch, M.P., McKee, A.C., Wald, L.L., et al. (2015). A computational atlas of the
847   hippocampal formation using ex vivo , ultra-high resolution MRI: Application to adaptive
848   segmentation of in vivo MRI. NeuroImage *115*, 117–137.

849 Jenkinson, M., Bannister, P., Brady, M., and Smith, S. (2002). Improved Optimization for the
850   Robust and Accurate Linear Registration and Motion Correction of Brain Images.
851   NeuroImage *17*, 825–841.

852 Jenkinson, M., Beckmann, C., Behrens, T., Woolrich, M., and Smith, S. (2012). FSL.
853   Neuroimage *62*, 782–790.

854 Johansen, J.P., Cain, C.K., Ostroff, L.E., and LeDoux, J.E. (2011). Molecular Mechanisms of
855   Fear Learning and Memory. Cell *147*, 509–524.

856 Johnson, J.D., McDuff, S.G.R., Rugg, M.D., and Norman, K.A. (2009). Recollection, Familiarity,
857   and Cortical Reinstatement: A Multivoxel Pattern Analysis. Neuron *63*, 697–708.

858 Josselyn, S.A., Köhler, S., and Frankland, P.W. (2015). Finding the engram. Nat Rev Neurosci
859   *16*, 521–534.

860 Keller, N.E., and Dunsmoor, J.E. (2020). The effects of aversive-to-appetitive
861   counterconditioning on implicit and explicit fear memory. Learning & Memory *27*, 12–19.

862 Kensinger, E.A., and Ford, J.H. (2021). Guiding the Emotion in Emotional Memories: The Role of
863   the Dorsomedial Prefrontal Cortex. Curr Dir Psychol Sci 0963721421990081.

864 Kim, H., Smolker, H.R., Smith, L.L., Banich, M.T., and Lewis-Peacock, J.A. (2020). Changes to
865   information in working memory depend on distinct removal operations. Nature
866   Communications *11*, 6239.

867 Klavir, O., Prigge, M., Sarel, A., Paz, R., and Yizhar, O. (2017). Manipulating fear associations
868   via optogenetic modulation of amygdala inputs to prefrontal cortex. Nature Neuroscience
869   *20*, 836–844.

870 Klein, A., Ghosh, S.S., Bao, F.S., Giard, J., Häme, Y., Stavsky, E., Lee, N., Rossa, B., Reuter,
871   M., Chaibub Neto, E., et al. (2017). Mindboggling morphometry of human brains. PLoS
872   Computational Biology *13*, e1005350.

873 Kriegeskorte, N., Goebel, R., and Bandettini, P. (2006). Information-based functional brain
874   mapping. PNAS *103*, 3863–3868.

875 Lacagnina, A.F., Brockway, E.T., Crovetti, C.R., Shue, F., McCarty, M.J., Sattler, K.P., Lim, S.C.,
876   Santos, S.L., Denny, C.A., and Drew, M.R. (2019). Distinct hippocampal engrams control
877   extinction and relapse of fear memory. Nature Neuroscience *22*, 753–761.

878 Lanczos, C. (1964). Evaluation of Noisy Data. Journal of the Society for Industrial and Applied
879   Mathematics Series B Numerical Analysis *1*, 76–85.

880 Lawrence, M.A. (2016). ez: Easy Analysis and Visualization of Factorial Experiments.

881 LeDoux, J.E., and Pine, D.S. (2016). Using neuroscience to help understand fear and anxiety: A
882   two-system framework. American Journal of Psychiatry *173*, 1083–1093.

883 Lenth, R. (2019). Emmeans: estimated marginal means Aka Least-Squares Means.
884   https://cran.r-project.org/package=emmeans.

885 Letzkus, J.J., Wolff, S.B.E., and Lüthi, A. (2015). Disinhibition, a Circuit Mechanism for
886   Associative Learning and Memory. Neuron *88*, 264–276.

887 Lissek, S., and van Meurs, B. (2015). Learning models of PTSD: Theoretical accounts and
888   psychobiological evidence. International Journal of Psychophysiology *98*, 594–605.

889 Liu, X., Ramirez, S., Pang, P.T., Puryear, C.B., Govindarajan, A., Deisseroth, K., and Tonegawa,
890   S. (2012). Optogenetic stimulation of a hippocampal engram activates fear memory recall.
891   Nature *484*, 381–385.

892 Luke, S.G. (2017). Evaluating significance in linear mixed-effects models in R. Behavior
893   Research Methods *49*, 1494–1502.

894 Marek, R., Jin, J., Goode, T.D., Giustino, T.F., Wang, Q., Acca, G.M., Holehonnur, R., Ploski,
895   J.E., Fitzgerald, P.J., Lynagh, T., et al. (2018). Hippocampus-driven feed-forward inhibition
896   of the prefrontal cortex mediates relapse of extinguished fear. Nature Neuroscience *21*,
897   384–392.

898 Maren, S., Phan, K.L., and Liberzon, I. (2013). The contextual brain: Implications for fear
899   conditioning, extinction and psychopathology. Nature Reviews Neuroscience *14*, 417–428.

900 Meyer, H.C., Odriozola, P., Cohodes, E.M., Mandell, J.D., Li, A., Yang, R., Hall, B.S., Haberman,
901   J.T., Zacharek, S.J., Liston, C., et al. (2019). Ventral hippocampus interacts with prelimbic
902   cortex during inhibition of threat response via learned safety in both mice and humans.
903   Proceedings of the National Academy of Sciences of the United States of America *116*,
904   26970–26979.

905 Milad, M.R., and Quirk, G.J. (2002). Neurons in medial prefrontal cortex signal memory for fear
906   extinction. Nature *420*, 70–74.

907 Milad, M.R., and Quirk, G.J. (2012). Fear Extinction as a Model for Translational Neuroscience:
908   Ten Years of Progress. Annual Review of Psychology *63*, 129–151.

909 Milad, M.R., Vidal-Gonzalez, I., and Quirk, G.J. (2004). Electrical stimulation of medial prefrontal
910   cortex reduces conditioned fear in a temporally specific manner. Behav Neurosci *118*,
911   389–394.

912 Milad, M.R., Quirk, G.J., Pitman, R.K., Orr, S.P., Fischl, B., and Rauch, S.L. (2007). A Role for
913   the Human Dorsal Anterior Cingulate Cortex in Fear Expression. Biological Psychiatry *62*,
914   1191–1194.

915 Moorman, D.E., and Aston-Jones, G. (2015). Prefrontal neurons encode context-based response
916   execution and inhibition in reward seeking and extinction. PNAS.

917 Mumford, J.A., Turner, B.O., Ashby, F.G., and Poldrack, R.A. (2012). Deconvolving BOLD
918   activation in event-related designs for multivoxel pattern classification analyses.
919   NeuroImage *59*, 2636–2643.

920 Mumford, J.A., Davis, T., and Poldrack, R.A. (2014). The impact of study design on pattern
921   estimation for single-trial multivariate pattern analysis. NeuroImage *103*, 130–138.

922 O'Reilly, R.C., and Rudy, J.W. (2001). Conjunctive representations in learning and memory:
923   Principles of cortical and hippocampal function. Psychological Review *108*, 311–345.

924 Pape, H.C., and Pare, D. (2010). Plastic synaptic networks of the amygdala for the acquisition,
925   expression, and extinction of conditioned fear. Physiological Reviews *90*, 419–463.

926 Pitman, R.K., Rasmusson, A.M., Koenen, K.C., Shin, L.M., Orr, S.P., Gilbertson, M.W., Milad,
927   M.R., and Liberzon, I. (2012). Biological studies of post-traumatic stress disorder. Nature
928   Reviews Neuroscience *13*, 769–787.

929 Polyn, S.M., Natu, V.S., Cohen, J.D., and Norman, K.A. (2005). Category-specific cortical activity
930   precedes retrieval during memory search. Science *310*, 1963–1966.

931 Poppenk, J., Evensmoen, H.R., Moscovitch, M., and Nadel, L. (2013). Long-axis specialization of
932   the human hippocampus. Trends in Cognitive Sciences *17*, 230–240.

933 Power, J.D., Mitra, A., Laumann, T.O., Snyder, A.Z., Schlaggar, B.L., and Petersen, S.E. (2014).
934   Methods to detect, characterize, and remove motion artifact in resting state fMRI.
935   NeuroImage *84*, 320–341.

Qin, C., Bian, X.-L., Wu, H.-Y., Xian, J.-Y., Cai, C.-Y., Lin, Y.-H., Zhou, Y., Kou, X.-L., Chang, L., Luo, C.-X., et al. (2021). Dorsal Hippocampus to Infralimbic Cortex Circuit is Essential for the Recall of Extinction Memory. Cerebral Cortex *31*, 1707–1718.

Raij, T., Nummenmaa, A., Marin, M.-F., Porter, D., Furtak, S., Setsompop, K., and Milad, M.R. (2018). Prefrontal Cortex Stimulation Enhances Fear Extinction Memory in Humans. Biological Psychiatry *84*, 129–137.

Rashid, A.J., Yan, C., Mercaldo, V., Hsiang, H.L., Park, S., Cole, C.J., De Cristofaro, A., Yu, J., Ramakrishnan, C., Lee, S.Y., et al. (2016). Competition between engrams influences fear memory formation and recall. Science *353*, 383–387.

Reijmers, L.G., Perkins, B.L., Matsuo, N., and Mayford, M. (2007). Localization of a Stable Neural Correlate of Associative Memory. Science *317*, 1230–1233.

Ressler, R.L., Goode, T.D., Kim, S., Ramanathan, K.R., and Maren, S. (2021). Covert capture and attenuation of a hippocampus-dependent fear memory. Nat Neurosci.

Ritchey, M., Wing, E.A., LaBar, K.S., and Cabeza, R. (2013). Neural Similarity Between Encoding and Retrieval is Related to Memory Via Hippocampal Interactions. Cerebral Cortex *23*, 2818–2828.

Satterthwaite, T.D., Elliott, M.A., Gerraty, R.T., Ruparel, K., Loughead, J., Calkins, M.E., Eickhoff, S.B., Hakonarson, H., Gur, R.C., Gur, R.E., et al. (2013). An improved framework for confound regression and filtering for control of motion artifact in the preprocessing of resting-state functional connectivity data. NeuroImage *64*, 240–256.

Saygin, Z.M., Kliemann, D., Iglesias, J.E., van der Kouwe, A.J.W., Boyd, E., Reuter, M., Stevens, A., Van Leemput, K., McKee, A., Frosch, M.P., et al. (2017). High-resolution magnetic resonance imaging reveals nuclei of the human amygdala: manual segmentation to automatic atlas. NeuroImage *155*, 370–382.

Seeley, W.W. (2019). The Salience Network: A Neural System for Perceiving and Responding to Homeostatic Demands. J. Neurosci. *39*, 9878–9882.

Senn, V., Wolff, S.B.E., Herry, C., Grenier, F., Ehrlich, I., Gründemann, J., Fadok, J.P., Müller, C., Letzkus, J.J., and Lüthi, A. (2014). Long-range connectivity defines behavioral specificity of amygdala neurons. Neuron *81*, 428–437.

Sierra-Mercado, D., Padilla-Coreano, N., and Quirk, G.J. (2011). Dissociable roles of prelimbic and infralimbic cortices, ventral hippocampus, and basolateral amygdala in the expression and extinction of conditioned fear. Neuropsychopharmacology *36*, 529–538.

Singmann, H., Bolker, B., and Westfall, J. (2015). Analysis of Factorial Experiments, package "afex."

Sotres-Bayon, F., Sierra-Mercado, D., Pardilla-Delgado, E., and Quirk, G.J. (2012). Gating of Fear in Prelimbic Cortex by Hippocampal and Amygdala Inputs. Neuron *76*, 804–812.

Staresina, B.P., Henson, R.N.A., Kriegeskorte, N., and Alink, A. (2012). Episodic reinstatement in the medial temporal lobe. Journal of Neuroscience *32*, 18150–18156.

974 Staudigl, T., Vollmar, C., Noachtar, S., and Hanslmayr, S. (2015). Temporal-pattern similarity
975   analysis reveals the beneficial and detrimental effects of context reinstatement on human
976   memory. Journal of Neuroscience *35*, 5373–5384.

977 Talairach, J. (1988). Co-Planar Stereotaxic Atlas of the Human Brain: 3-D Proportional System:
978   An Approach to Cerebral Imaging (Stuttgart ; New York: Thieme).

979 Taschereau-Dumouchel, V., Cortese, A., Chiba, T., Knotts, J.D., Kawato, M., and Lau, H. (2018).
980   Towards an unconscious neural reinforcement intervention for common fears.
981   Proceedings of the National Academy of Sciences *115*, 3470–3475.

982 Taschereau-Dumouchel, V., Cortese, A., Lau, H., and Kawato, M. (2020). Conducting decoded
983   neurofeedback studies. Social Cognitive and Affective Neuroscience.

984 Tovote, P., Fadok, J.P., and Lüthi, A. (2015). Neuronal circuits for fear and anxiety. Nat Rev
985   Neurosci *16*, 317–331.

986 Tronson, N.C., Schrick, C., Guzman, Y.F., Huh, K.H., Srivastava, D.P., Penzes, P., Guedea,
987   A.L., Gao, C., and Radulovic, J. (2009). Segregated Populations of Hippocampal Principal
988   CA1 Neurons Mediating Conditioning and Extinction of Contextual Fear. J. Neurosci. *29*,
989   3387–3394.

990 Tulving, E., and Thomson, D.M. (1973). Encoding specificity and retrieval processes in episodic
991   memory. Psychological Review *80*, 352–373.

992 Tustison, N.J., Avants, B.B., Cook, P.A., Zheng, Y., Egan, A., Yushkevich, P.A., and Gee, J.C.
993   (2010). N4ITK: Improved N3 bias correction. IEEE Transactions on Medical Imaging *29*,
994   1310–1320.

995 Twining, R.C., Lepak, K., Kirry, A.J., and Gilmartin, M.R. (2020). Ventral Hippocampal Input to
996   the Prelimbic Cortex Dissociates the Context from the Cue Association in Trace Fear
997   Memory. J. Neurosci. *40*, 3217–3230.

998 Vallat, R. (2018). Pingouin: statistics in Python. Journal of Open Source Software *3*, 1026.

999 Visser, R.M., Scholte, H.S., Beemsterboer, T., and Kindt, M. (2013). Neural pattern similarity
1000   predicts long-term fear memory. Nature Neuroscience *16*, 388–390.

1001 Wheeler, A.L., Teixeira, C.M., Wang, A.H., Xiong, X., Kovacevic, N., Lerch, J.P., McIntosh, A.R.,
1002   Parkinson, J., and Frankland, P.W. (2013). Identification of a Functional Connectome for
1003   Long-Term Fear Memory in Mice. PLOS Computational Biology *9*, e1002853.

1004 Ye, X., Kapeller-Libermann, D., Travaglia, A., Inda, M.C., and Alberini, C.M. (2017). Direct dorsal
1005   hippocampal–prelimbic cortex connections strengthen fear memories. Nature
1006   Neuroscience *20*, 52–61.

1007 Zhang, X., Kim, J., and Tonegawa, S. (2020). Amygdala Reward Neurons Form and Store Fear
1008   Extinction Memory. Neuron *105*, 1077-1093.e7.

1009   Zhang, Y., Brady, M., and Smith, S. (2001). Segmentation of brain MR images through a hidden
1010   Markov random field model and the expectation-maximization algorithm. IEEE
1011   Transactions on Medical Imaging *20*, 45–57.

1012

SUPPLEMENTARY RESULTS

Interactions in MTL univariate predicting mPFC reinstatement location.

In our analysis using univariate activity at the time of memory retrieval to predict the location of reinstatement in the mPFC, we observed several interactions with hippocampal subfield. For the pHC, there was a significant *pHC * CS type* interaction ($X^2_{(1)} = 11.2$, P = 8.3e-4), such that the slope of pHC activity was significantly more negative for CS+ compared to CS- (CS slope diff. = -1.53e-3, [-2.43e-3, -6.34e-4], P = 8.24e-4). In the body of the hippocampus, there was a significant *HC body * CS type * encoding context* interaction ($X^2_{(1)} = 5.46$, P = 0.019). Post-hoc contrasts revealed that for items encoded during conditioning, the slope for the CS+ was significantly more negative than the CS- (CS slope diff. = -2.68e-3, [-4.21e-3, -1.15e-3], P_{FDR} = 1.17e-3), while there was no difference in the slopes for extinction (CS slope diff. = -8.68e-5, [-1.63e-3, 1.46e-3], P_{FDR} = 0.91). There were no significant interactions in the aHC, BLA, or CeM. In sum, MTL univariate activity predicted more reinstatement in the dACC. This effect was stronger for all CS+ items in the pHC compared to CS-, and was selective for conditioning CS+ items in the body of the hippocampus.

Recognition memory does not influence reinstatement in the mPFC.

We additionally tested if reinstatement in our *a priori* ROIs differed as a function of memory strength. Recognition memory was included as a categorical predictor (e.g., "high-confidence hit" or "miss"). In the mPFC, there was no main effect of *memory accuracy* ($X^2_{(1)} = 0.024$, P = 0.89), and all interactions with this term were not significant (all Ps ≥ 0.14). A similar pattern emerged in the amygdala, with only a trending main effect of *memory accuracy* ($X^2_{(1)} = 3.08$, P = 0.08) and no significant interactions (all Ps ≥ 0.07). In the hippocampus, we again observed a trending main effect of *memory accuracy* ($X^2_{(1)} = 3.47$, P = 0.06), as well as several significant higher order interactions (*memory accuracy * CS type * encoding context*: $X^2_{(2)} = 6.26$, P = 0.044; *memory*

1037   *accuracy * CS type * subfield*: $X^2_{(2)}$ = 6.69, P = 0.035; *memory accuracy * encoding context **

1038   *group*: $X^2_{(2)}$ = 11.8, P = 0.003). Thus, recognition memory did not influence reinstatement in the

1039   mPFC and amygdala. Recognition memory influencing reinstatement in the hippocampus is

1040   consistent with this structure's role in episodic retrieval.

1041

Searchlight Clusters

Group	Encoding context	Label (hemisphere)	MNI coor. peak	Size in voxels (3mm^3)
Healthy	Acquisition	Inferior frontal gyrus (R)	33, 9, 27	741
		Superior frontal gyrus (L)	-6. 18, 51	608
		Middle frontal gyrus (L)	-39, 33, 15	414
		Angular gyrus (L)	33, -57, 36	308
		Insula (L)	-27, 24, -6	280
		Inferior frontal gyrus (L)	-45, 3, 21	178
		Precuneus (L)	-9, -66, 42	175
		Inferior parietal lobule (R)	30, -54, 42	117
		Cerebellar tonsil (R)	36, -63, -45	40
		Cerebellar tonsil (L)	-33, -60, -33	32
		Medial frontal gyrus (L)	-15, 48, -3	25
		Precuneus (R)	12, -75, 42	25
		Middle temporal gyrus (L)	-57, -51, -6	22
	Extinction	Medial frontal gyrus (L)	-3, 51, 0	191
		Precuneus (L)	-6, -63, 27	113
		Angular gyrus (L)	-39, -75, 36	69
		Angular gyrus (R)	42, -69, 30	44

		Middle temporal gyrus (R)	63, 0, -24	26
ptsd	Acquisition	Superior frontal gyrus (R)	-6, 18, 51	326
		Insula (L)	-33, 24, 9	214
		Insula (R)	30, 24, -6	201
		Precuneus (L)	-18, -66, 48	119
		Supramarginal gyrus (L)	-54, -48, 27	62
		Culmen / Parahippocampal gyrus (L)	-30, -51, -24	61
		Inferior frontal gyrus (R)	45, 6, 24	52
		Middle frontal gyrus (L)	-51, -3, 39	52
		Fusiform gyrus (L)	-57, -63, -12	29
		Precentral gyrus (L)	-42, -3, 51	23
		Middle frontal gyrus (L)	-42, 24, 24	22
		Superior temporal gyrus (L)	-51, -54, 15	20
	Extinction	Cuneus (L)	-6, -75, 30	42
		Insula (R)	36, 30, 3	34
		Insula (L)	-39, 27, 0	25

1043

1044   **Supplementary Table 1.** Whole-brain searchlight results. Clusters correspond to significant CS+

1045   – CS- reinstatement. Coordinates refer to the peak voxel in each cluster. Anatomical labels were

1046   derived from the Talairach-Tournoux Atlas.

1047